





Cite this: *Nanoscale*, 2018, **10**, 6343

Controllable rotational inversion in nanostructures with dual chirality†

Lu Dai,  ^{a,e} Ka-Di Zhu, ^b Wenzhong Shen, ^b Xiaojiang Huang, ^c Li Zhang  ^{*d} and Alain Goriely^e

Chiral structures play an important role in natural sciences due to their great variety and potential applications. A perversion connecting two helices with opposite chirality creates a dual-chirality helical structure. In this paper, we develop a novel model to explore quantitatively the mechanical behavior of normal, binormal and transversely isotropic helical structures with dual chirality and apply these ideas to known nanostructures. It is found that both direction and amplitude of rotation can be finely controlled by designing the cross-sectional shape. A peculiar rotational inversion of overwinding followed by unwinding, observed in some gourd and cucumber tendril perversions, not only exists in transversely isotropic dual-chirality helical nanobelts, but also in the binormal/normal ones when the cross-sectional aspect ratio is close to 1. Beyond this rotational inversion region, the binormal and normal dual-chirality helical nanobelts exhibit a fixed directional rotation of unwinding and overwinding, respectively. Moreover, in the binormal case, the rotation of these helical nanobelts is nearly linear, which is promising as a possible design for linear-to-rotary motion converters. The present work suggests new designs for nanoscale devices.

Received 4th December 2017,

Accepted 19th February 2018

DOI: 10.1039/c7nr09035h

rsc.li/nanoscale

Introduction

Chiral structures play a prominent role in many natural and technology processes ranging from protein configuration,^{1,2} development, to nanomechanics.^{3,4} Helices with given chirality are critical elements in a host of applications at the nanoscale as they provide simple springs and, more importantly, a direct way to convert linear motion to rotational motion and rotational motion to linear motion. An example of this conversion process is the functionalized helical micro-/nano-swimmers, which are optimized to have a pure rotation translation along their helical axis.⁵ Such swimming robots are a promising tool for single-cell-targeted drug, DNA, and enzyme delivery *in vitro* as well as *in vivo*.^{6–8} Conversely, in the transformation from linear motion to rotational motion, elasticity plays a key role. Yet, the linear regime of simple springs is limited due to torsional lock-up: as a spring is pulled in simple extension, it quickly stiffens due to its inability to untwist without

one of the ends turning. An elegant solution to this mechanical problem, first proposed in ref. 9, is to design a “twistless spring” by using filaments that exhibit both left and right chirality connected by a short inversion called a “perversion”, a term introduced by the mathematician J. B. Listing to describe the reversal of one chiral structure into another.¹⁰

This kind of helix with dual chirality was first described in plant physiology in a letter of André-Marie Ampère.^{11,12} Then Charles Darwin pointed out that a tendril with perversion creates a twistless flexible elastic structure connecting a climbing plant to its support¹³ (see ref. 14 for historical details). Inspired by the tendrils, it is found that an inverted structure can be created through an instability in a filament with intrinsic curvature under tension by either decreasing the tension or increasing the intrinsic curvature.¹⁵ The structure emerging has dual chirality and, due to its particular cancellation of twist, has an excellent mechanical behavior of tension-extension close to an ideal linear Hookean response.⁹ Moreover, a helical structure with dual chirality has a remarkable rotational property during extension: it is reported that some young and old cucumber tendril coils unwind and overwind with axial extension, respectively.¹⁶

There is yet another peculiar rotational behavior of helices with dual chirality. As presented in Fig. 1(a), we find that some young gourd and cucumber tendrils, always overwind in the beginning of axial extension, and then unwind when elongation is further increased (ESI Movie S1† for gourd and ESI Movie S2† for cucumber). In this experiment, we use a slow

^aSchool of Mathematics and Physics, Suzhou University of Science and Technology, Suzhou 215009, China. E-mail: dailu.1106@aliyun.com

^bDepartment of Physics and Astronomy, Shanghai Jiao Tong University, 800 Dongchuan Road, Minhang District, Shanghai 200240, China

^cCollege of Science, Donghua University, Shanghai 201620, China

^dDepartment of Mechanical and Automation Engineering, The Chinese University of Hong Kong, Shatin NT, Hong Kong SAR, China. E-mail: lizhang@mae.cuhk.edu.hk

^eMathematical Institute, University of Oxford, Oxford OX2 6GG, UK

†Electronic supplementary information (ESI) available. See DOI: 10.1039/c7nr09035h

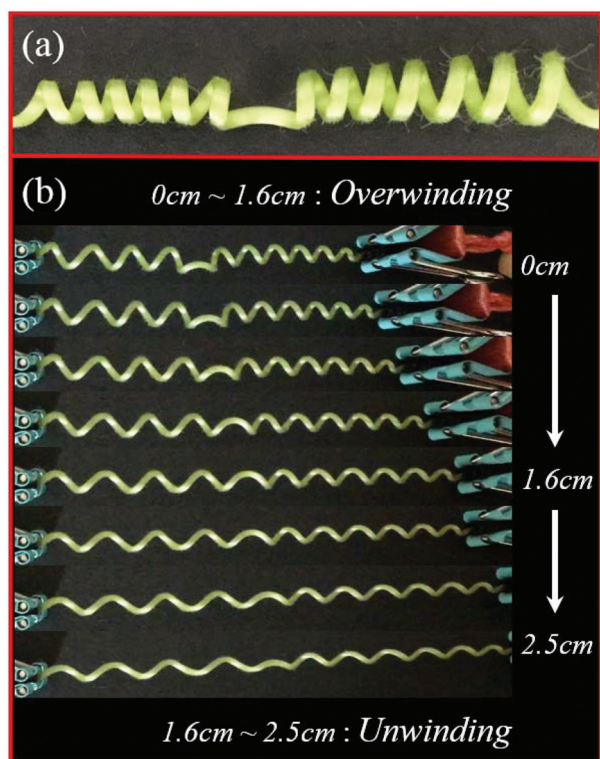


Fig. 1 (a) A gourd tendril coil. (b) The rotation states of a gourd tendril coil during an axial loading process.

axial loading (of about 0.3 cm s^{-1} and 0.05 coil length per second) so that the tendril is in a quasi-static equilibrium at all times. Fig. 1(b) displays the rotation states of a gourd tendril coil during axial loading. The gourd tendril coil first overwinds when the elongation increases to 1.6 cm , and then unwinds during the rest of the loading process. Interestingly, this non-monotonic behavior, known as the twist-stretch coupling, also exists in the microscopic single-chirality DNA molecules.^{17,18} As extension increases, each point on the DNA rotates around the axis by first overwinding around it (adding a further twist in the spring) and then unwinding it (hence removing the twist).^{19,20}

Helical rods can be classified into three types: transversely isotropic helices (with rotationally invariant sections such as the squares and circles), and normal and binormal helices with non-rotational invariant sections (such as the rectangular or elliptical cross-sections).²¹ In this paper, we study the rotational and extensional behaviour of nanohelices with dual chirality that have either transverse isotropy or are composed of normal and binormal helices (referred to here as “nanobelts”). A binormal dual-chirality nanobelt can be fabricated *via* a strain-driven self-rolling mechanism.²² These structures are known to unwind during the axial extension.²³ A normal dual-chirality nanobelt can be realized by 3D direct laser writing, which has been used to print single normal nanohelices.²⁴ A transversely isotropic cellulosic micro/nano-fiber with dual-chirality can be produced by electrospinning in

liquid crystalline solutions.²⁵ Under electronic beam exposure, a suspended cellulosic fiber exhibits unwinding and overwinding behavior.²⁶ Therefore, it is of great practical significance to provide an accurate theoretical description of the mechanical properties for the normal, binormal, and isotropic dual-chirality nanohelices.

In this paper, we provide a theoretical basis for the mechanics of normal, binormal, and transversely isotropic helical nanostructures with dual chirality by employing a general extensible rod theory. We show that by modifying the shape of the cross-section, one can tune the rotational properties of direction and amplitude of these structures to obtain a linear rotational response under extension. In particular, a controllable rotational inversion can be obtained from the dual-chirality nanohelices of transverse isotropy, as well as of normal/binormal in a narrow region defined by the aspect ratio of the rectangular cross-section.

Modeling

The general set-up of our model is shown in Fig. 2(a)–(d). We assume that a rod with width w and thickness t ($w > t$) rolls up into a uniform helical structure with dual chirality H_{PI} , with radius a_0 , pitch b_0 , and N_0 helical turns. This structure is slowly loaded by an axial force F , while the ends are prevented from rotating. In this process, the structure is transformed into another helical structure with dual chirality H_{PF} , with a radius a , pitch b , and N helical turns. The director basis D_i ($i = 1, 2, \text{ and } 3$) consisting of the normal, binormal, and tangent vectors of H_{PI} and the director basis d_i of H_{PF} are described by their Euler angles $(\varphi_0, \theta_0, \psi_0)$ and (φ, θ, ψ) , respectively.^{27,28} We

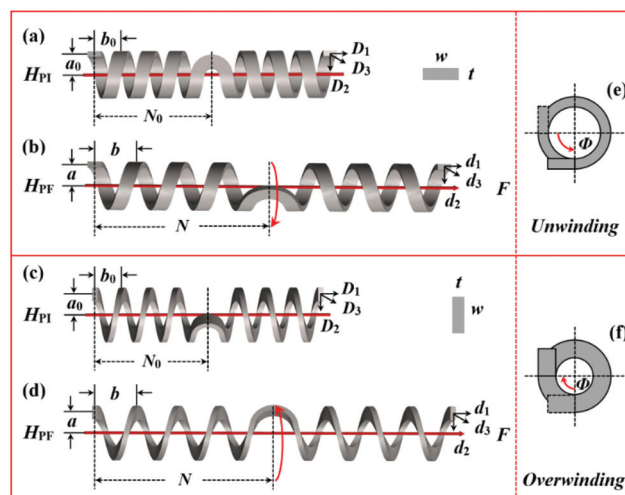


Fig. 2 Schematic illustration of the dual-chirality nanohelices with the rectangular cross-section H_{PI} of (a) binormal and (c) normal nanohelices. The configurations of the corresponding elongated nanohelix with the dual chirality H_{PF} of (b) binormal and (d) normal after loading by the tensile force F along the helical axes. The corresponding cross-sections of the whole (e) binormal and (f) normal nanohelices with dual chirality at the mirror symmetry axes.

can use the mirror symmetry of these structures to our advantage by modeling their response as two helical springs where one end is free to rotate. We follow the terminology of ref. 29 and denote S to be the arc length along the fixed reference configuration H_{PI} and s the arc length along the deformed configuration H_{PF} . The corresponding derivatives are defined by $\widehat{(\cdot)} = \partial(\cdot)/\partial S$ and $\dot{(\cdot)} = \partial(\cdot)/\partial s$. Based on the general elastic rod theory, the derivation processes for the radii a_0 and a , pitches b_0 and b as well as the loading force F , the torque along the helix axis M of each helix of H_{PF} are the same as those of a loaded helical structure with two ends restricted from winding,²⁹ except that in this situation $\dot{\psi} \neq \dot{\psi}_0$ due to the fact that $N \neq N_0$. Therefore, the radius and pitch are given by:

$$a_0 = \frac{\sin \theta_0}{\dot{\psi}_0}, \quad b_0 = \frac{2\pi \cos \theta_0}{\dot{\psi}_0}. \quad (1)$$

$$a = \frac{1}{\dot{\psi}} \left[\left(\frac{F}{E_3} \cos \theta + 1 \right) - \frac{F}{E_1} \cos \theta \right] \sin \theta, \quad (2)$$

$$b = \frac{2\pi}{\dot{\psi}} \left[\frac{F}{E_1} \sin^2 \theta + \left(\frac{F}{E_3} \cos \theta + 1 \right) \cos \theta \right].$$

For a helix with N helical turns of H_{PF} , the number of turns N is given by:³⁰

$$N = \frac{\dot{\psi}}{2\pi} l_0, \quad (3)$$

where $l_0 = N_0 \sqrt{(2\pi a_0)^2 + b_0^2}$ is the length of the coil wire of H_{PI} .

The balance of force and moment connect the axial force F and axial moment M to the deformed shape of the helical structure by the following two relations:

$$\left(\frac{1}{E_3} - \frac{1}{E_1} \right) \cos \theta \sin \theta F^2 + \sin \theta F - C(\dot{\psi} \cos \theta - \dot{\psi}_0 \cos \theta_0) \dot{\psi} \sin \theta$$

$$+ EI_1 [1 - (1 - \Delta) \delta_{i2}] (\dot{\psi} \sin \theta - \dot{\psi}_0 \sin \theta_0) \dot{\psi} \cos \theta = 0, \quad (4)$$

$$M = EI_1 [1 - (1 - \Delta) \delta_{i2}] (\dot{\psi} \sin \theta - \dot{\psi}_0 \sin \theta_0) \sin \theta$$

$$+ C(\dot{\psi} \cos \theta - \dot{\psi}_0 \cos \theta_0) \cos \theta, \quad (5)$$

where $\Delta \equiv I_2/I_1$, $i = 1$ for a normal ($i = 2$ for a binormal) helix and $I_1 = w^3 t/12$ and $I_2 = wt^3/12$ are the moments of inertia of a rectangular cross-section. δ_{i2} is the Kronecker delta. $E_1 = KGtw$, $E_3 = Etw$ and $C = 4GI_1 I_2 / (I_1 + I_2)$ according to the scaled torsional stiffness.³¹ K is the Timoshenko shear coefficient and related to Poisson's ratio ν through $K = (5 + 5\nu)/(6 + 5\nu)$.³² E and $G = E/2(1 + \nu)$ are the Young's and shear moduli of the material, respectively.³³

It is of particular interest to look at the case $M = 0$ for a loaded helical structure, corresponding to the case where one end is free to rotate. From (4), we obtain

$$\dot{\psi} = \frac{EI_1 [1 - (1 - \Delta) \delta_{i2}] \sin \theta_0 \sin \theta + C \cos \theta_0 \cos \theta}{EI_1 [1 - (1 - \Delta) \delta_{i2}] \sin^2 \theta + C \cos^2 \theta} \dot{\psi}_0. \quad (6)$$

Fig. 2(e) and (f) are the cross-sections of the binormal and normal helical structures with dual chirality at the mirror symmetry axes, respectively. The perversions before and after

loading are presented by the solid and dashed rectangles, respectively. Φ is the rotation angle of the free end of the helical structure, *i.e.*, the rotation angle of perversion:

$$\Phi = 360^\circ \times (N - N_0). \quad (7)$$

The spring constant of each helical structure of H_{PF} is deduced from (1)–(4), in the linear limit $h = dF/d(Nb)$:

$$h_s = -\frac{P_1 P_3}{2(P_1 P_4 + P_2)},$$

$$P_1 = \left(\frac{1}{E_3} - \frac{1}{E_1} \right) \left(\sin \theta - \frac{\cos^2 \theta}{\sin \theta} \right) F^2 - \frac{\cos \theta}{\sin \theta} F + \frac{Q_6}{2 \cos \theta} \left(\sin \theta - \frac{\cos^2 \theta}{\sin \theta} \right) \dot{\psi}^2$$

$$+ \left[2 \sin \theta \frac{Q_6(Q_4 Q_5 + Q_3 Q_6)}{Q_4^2} - \frac{Q_3}{\sin \theta} \right] \dot{\psi}_0 \dot{\psi}$$

$$+ \sin \theta \frac{Q_5(Q_4 Q_5 + Q_3 Q_6)}{Q_4^2} \dot{\psi}_0^2, \quad P_2 = Q_2 \sin \theta, \quad P_3 = \frac{1}{Q_2 l_0},$$

$$P_4 = -\frac{Q_1}{Q_2},$$

where,

$$Q_1 = \left(\frac{1}{E_3} - \frac{1}{E_1} \right) \cos^2 \theta + \frac{1}{E_1},$$

$$Q_2 = 2 \left(\frac{1}{E_3} - \frac{1}{E_1} \right) F \cos \theta + 1,$$

$$Q_3 = EI_1 [1 - (1 - \Delta) \delta_{i2}] \sin \theta_0 \sin \theta + C \cos \theta_0 \cos \theta, \quad (8)$$

$$Q_4 = EI_1 [1 - (1 - \Delta) \delta_{i2}] \sin^2 \theta + C \cos^2 \theta,$$

$$Q_5 = -EI_1 [1 - (1 - \Delta) \delta_{i2}] \sin \theta_0 \frac{\cos \theta}{\sin \theta} + C \cos \theta_0,$$

$$Q_6 = 2(EI_1 [1 - (1 - \Delta) \delta_{i2}] - C) \cos \theta.$$

Since the two opposite-handed helical structures of H_{PF} are connected in series, the spring constant of H_{PF} is:

$$h_p = \frac{h_s}{2}. \quad (9)$$

Using (1)–(9), we can obtain the radius a , pitch b , N helical turns and the spring constant h_p of the helical structure with dual chirality H_{PF} from the known radius a_0 , pitch b_0 , the number of turns in each helix N_0 of H_{PI} and the loading force F .

Results

In order to understand the mechanical behavior of nanohelices with dual chirality, we analyze a rolled-up nanohelix. The strain-induced self-scrolling mechanism is a highly controllable fabrication method that allows to create dual-chirality nanohelices with adjustable helix angles. Fig. 3(a) shows that a binormal dual-chirality nanohelix is fabricated from the symmetric V-shaped SiGe/Si/Cr nanobelt, which leads to a left and right-handed arm having the same geometry parameters. The 8/10 nm thick SiGe/Si hetero-structures with approximately 40% Ge in the SiGe layer were *epi*-grown by chemical vapor deposition (CVD) on the Si(110) substrates. The 13 nm thick amorphous Cr layers were deposited by e-beam evaporation. The details of the SiGe/Si/Cr pattern fabrication and the wet

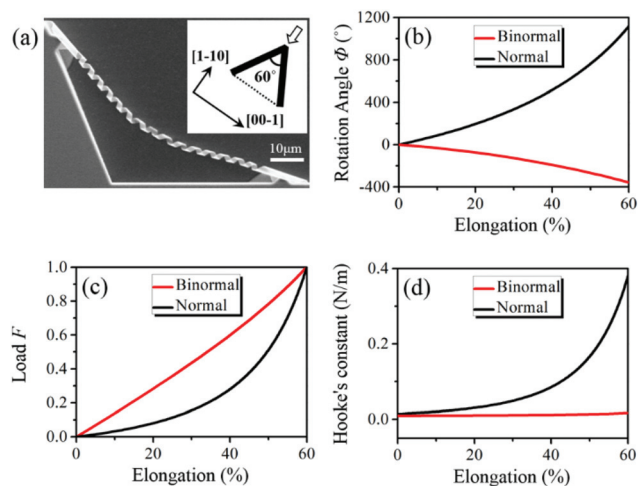


Fig. 3 (a) SEM image of a binormal SiGe/Si/Cr dual-chirality helical nanohelix formed by a symmetric V-shaped mesa with both ends fixed to the Si(110) substrate. The inset shows the mesa design and the rolling direction of the helix as indicated with a hollow arrow. (b) Rotation angle of perversion, (c) axial load, and (d) spring constant versus axial elongation of the fabricated binormal nanohelix as well as a normal one with the same parameters.

chemical etching for the subsequent underetching are described elsewhere.^{22,34} The binormal nanohelix with dual chirality has a radius $a_0 = 1.18 \mu\text{m}$, pitch $b_0 = 4.47 \mu\text{m}$ and $N_0 = 6$. The insets present the V-shaped mesa designs of 60°, as well as the rolling direction of the helix as indicated with a white arrow. In the following calculations, we use the parameters of this fabricated SiGe/Si/Cr nanohelix, including the area of the cross-section, the radius, the pitch, the number of turns, and the material parameters. (As presented in ESI Fig. S1,† we provide another SiGe/Si/Cr binormal dual-chirality nanohelix as an example to quantitatively analyse the mechanical properties of rotation.)

By pulling both ends of a nanohelix with dual chirality, the central part of the perversion performs a rotary motion,^{16,23} which makes it a perfect material for a linear-to-rotary motion nanometer converter. Fig. 3(b) presents the rotation angle of perversion versus the axial elongation for the fabricated binormal SiGe/Si/Cr nanohelix with a red curve. The modeling results are deduced from (1)–(6) with the geometry parameters as well as the material parameters of $E_{\text{SiGe}} = 161.2 \text{ GPa}$, $\nu_{\text{SiGe}} = 0.27$,³⁴ $E_{\text{Si}} = 168.9 \text{ GPa}$, $\nu_{\text{Si}} = 0.36$,^{35,36} and $E_{\text{Cr}} = 377 \text{ GPa}$, $\nu_{\text{Cr}} = 0.31$.³⁷ The SiGe/Si/Cr binormal nanohelix unwinds while extending axially and rotates 358°, *ca.* 1 turn, when it is stretched to 160% of its original length. The unwinding rotation direction of this binormal nanohelix is marked with red arrows in Fig. 2(b) and (e). Remarkably, during the first turn, the rotation angle and the axial elongation are very close to a linear relation and the corresponding linear-to-rotary ratio is approximately 597° per unit length. This kind of linear rotation has been observed in a loading experiment of the SiGe/Si nanohelix.²³ As shown in Fig. 3(b), we also study the linear-to-rotary motion of a normal dual-chirality helical nano-

helix with the same parameters as those of the binormal SiGe/Si/Cr nanohelix. It is interesting to compare the binormal and normal nanohelices. The normal helix overwinds in the reverse direction and has a larger amplitude of rotation: it overwinds to 1116°, *i.e.* 3.1 turns, when the elongation reaches 60% (see Fig. 2(d) and (f)). It is notable that the normal helix deviates from the linear behavior in the elastic regime by only 10%. Therefore, the binormal nanohelices with dual chirality are a more appropriate choice for a linear-to-rotary motion nanometer converter in 3-D scanning probe microscopes or microgoniometers.

Fig. 3(c) illustrates the axial load versus elongation of the SiGe/Si/Cr binormal nanohelix with dual chirality and the corresponding normal helix in the region of 60% elongation, using (1)–(6). All the loading forces of binormal/normal nanohelices are divided by their respective maximum loading force in this region. We observe that the binormal nanohelix with dual chirality is stretched linearly with the loading force, unlike the normal helix.

We further describe in Fig. 3(d) how the spring constant depends on the elongation for both the SiGe/Si/Cr binormal and normal nanohelices with dual chirality in the region of 60% elongation, obtained using (7) and (8). The spring constant of the binormal nanohelix remains constant with a value of 0.012 N m^{-1} , which will facilitate the actuation of the motion converters. A spring constant of the same magnitude of order as 0.012 N m^{-1} has been measured in a SiGe/Si nanohelix.²³ In contrast, the normal nanohelix has a wide spring constant change from 0.014 N m^{-1} to 0.379 N m^{-1} , increasing 27 times under load. Therefore, we conclude that binormal nanohelices with dual chirality are more appropriate for high-resolution force measurement in nanoelectromechanical systems.

Since normal and binormal helices exhibit opposite rotary motions, what is the behavior of a transversely isotropic rod (created with a square or circular section)? Fig. 4(a) presents the rotation angle Φ of perversion versus the axial elongation for a transversely isotropic dual-chirality nanohelix with a square cross-section, derived from (1)–(7). In the loading process, the dual-chirality nanohelix with a square cross-section exhibits the rotational inversion: it first overwinds to 18°, *i.e.* 0.05 turns, when the elongation increases to 22%; then unwinds to 73°, *i.e.* 0.2 turns, when the elongation increases to 60% as shown in Fig. 4. Therefore, the rotation property of transversely isotropic dual-chirality nanohelices is displayed in different stages with different axial loads. Interestingly, this rotational inversion is similar to the one we observed in some gourd and cucumber tendrils (Fig. 1(b)). We note that all transversely isotropic rods will behave, as expected from the general theory and illustrated for a fabricated SiGe/Si/Cr nanohelix transforms with a circular cross-section (inset of Fig. 4(a)).

We further identify the range of the aspect ratio of the rectangular cross-section $\eta = w/t$ for the nanohelices with dual chirality that acquires the characteristic of rotational inversion. Fig. 4(c) shows how the rotation direction of perversion

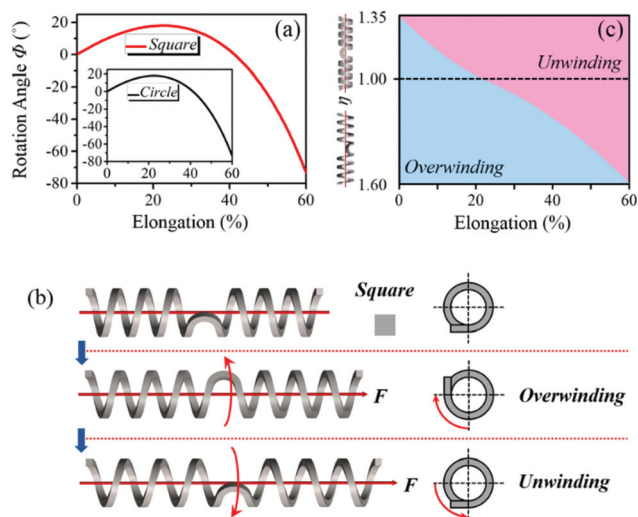


Fig. 4 (a) Rotation angle ϕ of perversion versus axial elongation of the transversely isotropic dual-chirality nanohelices with square and circle cross-sections. (b) The rotational inversion process of a transversely isotropic dual-chirality nanohelix with the square cross-section, as well as its cross-section at the mirror symmetry axis. (c) The rotational inversion region defined by the aspect ratio of the rectangular cross-section η .

depends on η during the axial loading, based on (1)–(6). The dashed line of $\eta = 1$ represents the dual-chirality nanohelix with a square cross-section. The areas above and below the dashed line indicate the binormal and normal helical nanohelices with dual chirality, respectively. We note that the rotational inversion of overwinding followed by unwinding only happens in a very narrow region of $1 < \eta < 1.35$ for the binormal nanohelix with dual chirality and $1 < \eta < 1.6$ for the normal one.

Fig. 5 illustrates the rotation angle versus the elongation for $1 \leq \eta \leq 50$. The area between the two red dotted dashed curves of $\eta = 1.35$ and $\eta = 1.6$ is the region of rotational inversion as shown in Fig. 5(b); while the rest is the region of unidirectional rotation. A binormal dual-chirality nanohelix with $\eta \geq 1.35$ or a normal one with $\eta \geq 1.6$ will only unwind or wind, respectively, during the whole loading process. According to the colourmap,

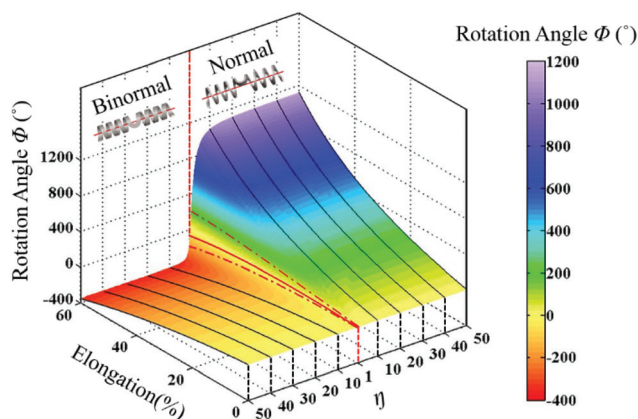


Fig. 5 Rotation angle perversion versus elongation for $1 \leq \eta \leq 50$.

the uni-directional rotational behavior of perversion is affected significantly by the aspect ratio η when it is smaller than 10: for an elongation of 60%, the rotation angle varies from 186° to 352° with η increasing from 1.35 to 10 (binormal), and from 198° to 1049° with η increasing from 1.6 to 10 (normal). However, when the value of η exceeds 10, the relationship between the elongation and the rotation angle is close to linear for the binormal nanohelices with dual chirality. We see from this analysis that both direction and amplitude of rotation can be finely adjusted by changing the shape of the cross-section for a dual-chirality helical micro-/nano-structure made out of the determined material.

Conclusions

We have shed light on the important mechanical properties of helical nanostructures with dual chirality by using a general elastic rod theory that include bending, torsion, twist, extension, and shear. Our model was used to analyze the behavior of a SiGe/Si/Cr dual-chirality nanohelix. It reveals that the transversely isotropic nanohelix always overwinds initially in axial extension, and then unwinds for larger tension. We also observe that this kind of rotational inversion exists in some gourd and cucumber tendrils. Importantly, we find that a rotational inversion region defined by the aspect ratio of rectangular cross-sections η is given by: $1 < \eta < 1.35$ and $1 < \eta < 1.6$ for binormal and normal nanohelices with dual chirality, respectively. Beyond this narrow region, the binormal and normal nanohelices with dual chirality only unwind and overwind, respectively. It is found that for the normal dual chirality nanohelices, the rotation angle of perversion, the loading force and spring constant all increase substantially and nonlinearly with extension; while binormal dual chirality nanohelices with $\eta > 10$ rotate and stretch both linearly with loading force, and a spring constant for $\eta = 50$ as small as 0.012 N m^{-1} . Therefore, these remarkable mechanical properties suggest that binormal nanohelices with dual chirality would be excellent linear-to-rotary motion converters. This work provides a theoretical framework for further experimental investigation on helical structures with dual chirality, as well as their applications in novel helical devices and micro-/nano-electromechanical systems.

Conflicts of interest

There are no conflicts to declare.

Acknowledgements

This work was supported by the National Natural Science Foundation of China under Grant No. 11547042, 11274230, 11574206, 11474201 and 11674225. L. Z. thanks the financial support, by the Early Career Scheme (ECS) with the Project No. 439113, from the Research Grants Council (RGC) of Hong Kong SAR, and the Science, Technology and Innovation Committee of Shenzhen Municipality (SZSTI)

Fundamental Research and Discipline Layout project (No. JCYJ20170413152640731). We thank Qianqian Wang (The Chinese University of Hong Kong) for simulated three-dimensional helices.

References

- 1 P. Cluzel, A. Lebrun, C. Heller, R. Lavery, J. L. Viovy, D. Chatenay and F. Caron, *Science*, 1996, **271**, 792–794.
- 2 B. L. Feringa and R. A. Delden, *Angew. Chem., Int. Ed.*, 1999, **38**, 3418–3438.
- 3 R. Dreyfus, J. Baudry, M. L. Roper, M. Fermigier, H. A. Stone and J. Bibette, *Nature*, 2005, **437**, 862–865.
- 4 M. G. L. van den Heuvel and C. Dekker, *Science*, 2007, **317**, 333–336.
- 5 L. Zhang, J. J. Abbott, L. X. Dong, K. E. Peyer, B. E. Kratochvil, H. X. Zhang, C. Bergeles and B. J. Nelson, *Nano Lett.*, 2009, **9**, 3663–3667.
- 6 S. Tottori, L. Zhang, F. Qiu, K. K. Krawczyk, A. F. Obregón and B. J. Nelson, *Adv. Mater.*, 2012, **24**, 811–816.
- 7 S. Tottori, L. Zhang, K. E. Peyer and B. J. Nelson, *Nano Lett.*, 2013, **13**, 4263–4268.
- 8 F. M. Qiu, S. Fujita, R. Mhanna, L. Zhang, B. R. Simona and B. J. Nelson, *Adv. Funct. Mater.*, 2015, **25**, 1666–1671.
- 9 T. McMillen and A. Goriely, *J. Nonlinear Sci.*, 2002, **12**, 241–281.
- 10 J. B. Listing, *Vorstudien über topologie*, Göttinger Studien, 1847, vol. I, pp. 811–875.
- 11 A. P. Candolle, *Organographie végétale*, Chez Deterville, Paris, 1827.
- 12 A. P. Candolle, *Physiologie végétale*, Béchét Jeune, Paris, 1832.
- 13 Ch. Darwin, *The movements and habits of climbing plants*, John Murray, London, 1865.
- 14 A. Goriely, *The mathematics and mechanics of biological growth*, Springer, New York, 2017.
- 15 A. Goriely and M. Tabor, *Phys. Rev. Lett.*, 1998, **80**, 1564–1567.
- 16 S. J. Gerbode, J. R. Puzey, A. G. McCormick and L. Mahadevan, *Science*, 2012, **337**, 1087–1091.
- 17 J. Gore, Z. Bryant, M. Nollmann, M. U. Le, N. R. Cozzarelli and C. Bustamante, *Nature*, 2006, **442**, 836–839.
- 18 T. Lionnet, S. Joubaud, R. Lavery, D. Bensimon and V. Croquette, *Phys. Rev. Lett.*, 2006, **96**, 178102.
- 19 J. W. Miller, *Phys. Rev.*, 1902, **14**, 129–148.
- 20 B. Durickovic, A. Goriely and J. H. Maddocks, *Phys. Rev. Lett.*, 2013, **111**, 108103.
- 21 A. Goriely and P. Shipman, *Phys. Rev. E: Stat. Phys., Plasmas, Fluids, Relat. Interdiscip. Top.*, 2000, **61**, 4508–4517.
- 22 L. Zhang, E. Deckhardt, A. Weber, C. Schonenberger and D. Grutzmacher, *Nanotechnology*, 2005, **16**, 655–663.
- 23 L. X. Dong, L. Zhang, B. E. Kratochvil, K. Shou and B. J. Nelson, *J. Microelectromech. Syst.*, 2009, **18**, 1047–1053.
- 24 T. Y. Huang, M. S. Sakar, A. Mao, A. J. Petruska, F. Qiu, X. B. Chen, S. Kennedy, D. Mooney and B. J. Nelson, *Adv. Mater.*, 2015, **27**, 6644–6650.
- 25 M. H. Godinho, J. P. Canejo, G. Feioa and E. M. Terentjev, *Soft Matter*, 2010, **6**, 5965–5970.
- 26 J. P. Canejo and M. H. Godinho, *Materials*, 2013, **6**, 1377–1390.
- 27 A. Goriely and M. Tabor, *Physica D*, 1997, **160**, 22–44.
- 28 A. B. Whitman and C. N. Desilva, *J. Elasticity*, 1974, **4**, 265–280.
- 29 L. Dai, L. Zhang, L. X. Dong, W. Z. Shen, X. B. Zhang, Z. Z. Ye and B. J. Nelson, *Nanoscale*, 2011, **3**, 4301–4306.
- 30 A. Goriely and M. Tabor, *Proc. R. Soc. London, Ser. A*, 1997, **453**, 2583–2601.
- 31 Z. C. Zhou, P. Y. Lai and B. Joos, *Phys. Rev. E: Stat. Phys., Plasmas, Fluids, Relat. Interdiscip. Top.*, 2005, **71**, 052801.
- 32 W. A. Fate, *J. Appl. Phys.*, 1975, **46**, 2375–2377.
- 33 S. P. Timoshenko and J. M. Gere, *Mechanics of Materials*, Van Nostrand, Princeton, 1972.
- 34 L. Zhang, E. Ruh, D. Grutzmacher, L. X. Dong, D. J. Bell, B. J. Nelson and C. Schonenberger, *Nano Lett.*, 2006, **6**, 1311–1317.
- 35 X. L. Li, *J. Phys. D: Appl. Phys.*, 2008, **41**, 193001.
- 36 J. J. Wortman and R. A. Evans, *J. Appl. Phys.*, 1965, **36**, 153–156.
- 37 S. V. Golod, V. Ya. Prinz, P. Wägli, L. Zhang, O. Kirfel, E. Deckhardt, F. Glaus, C. David and D. Grützmacher, *Appl. Phys. Lett.*, 2004, **84**, 3391–3393.